

# Numerical analysis of geodynamic evolution of the Earth based on a thermochemical model of the mantle convection

L. I. Lobkovsky

P. P. Shirshov Institute of Oceanology, RAS

V. D. Kotelkin

Mechanical–Mathematical Faculty of the Moscow State University

**Abstract.** Full-scale numerical modeling of the geodynamic evolution of the Earth throughout its existence is performed in terms of the thermochemical model of mantle convection proposed by the authors. Numerical modelling results are visualized in color and their detailed videorecord is presented. The global geodynamic process is clearly characterized by the presence of cycles of different lengths. Hydrodynamic pulsations associated with reorganizations of convective cells in the upper mantle correlate well with the geological cycles of Stille ( $\sim 30$  Myr). Moreover, the numerical experiments have shown that large avalanche-like flows of substance from the upper mantle into the lower mantle through their endothermic interface took place during the geodynamic evolution of the Earth; these impulsive downward flows significantly differ both quantitatively and qualitatively. In particular, impulsive flows of upper mantle substance into the lower mantle on a continental or regional scale (the so-called avalanches), also observable in our model, correspond in our interpretation to the geological cycles of Bertrand ( $\sim 170$  Myr). In addition, numerical experiments revealed the presence of basically new impulsive flows of upper mantle substance into the lower mantle on a planetary (global) scale that are referred to as overturns; about half of the upper mantle material is replaced by the material of the lower mantle over a relatively short time of the development of such an overturn. In our interpretation, the mantle overturns correlate with the Wilson cycles (700–900 Myr), which is evidence of their geodynamic nature and accounts for such major geological events as periodic assemblages and breakups of continent, the asymmetric structure of the Earth, and others. As the mantle cools during the evolution of the Earth, mantle overturns gradually attenuate and degenerate into mantle avalanches.

## Introduction

The mantle is the major layer of the Earth's structure and its physical state and convective motions control contemporary geodynamic processes and their effects in the past geological epochs. Therefore, their adequate description in

terms of mantle convection is of crucial importance for the evolution of the planet as a whole.

A convenient mathematical approach to the separation of the mantle layer from the global structure of the Earth and the separate examination of this layer consists in the specification of fixed boundary conditions independent of motions in the Earth's core. Since the Earth contains the metallic core with a large heat capacity, whose outer part is in the liquid state and can freely mix, convection in the mantle admits the classical formulation of the thermal convection problem [Rayleigh, 1916], assuming that temperatures at the upper and lower boundaries of the layer are constant and tangential stresses vanish at these boundaries.

Copyright 2004 by the Russian Journal of Earth Sciences.

Paper number TJE04144.

ISSN: 1681–1208 (online)

The online version of this paper was published 20 May 2004.

URL: <http://rjes.wdcb.ru/v06/tje04144/tje04144.htm>

The classical approach has composed the independent, purely thermal direction of research, whose main results were obtained by American and Canadian researchers [Bercovici *et al.*, 1989; Glatzmaier *et al.*, 1990; Solheim and Peltier, 1994; Tackley *et al.*, 1993]. Original results obtained in terms of a thermal convection model complemented with floating continents were obtained by Russian researchers [Trubitsyn and Rykov, 1998, 2000].

Moreover, the classical approach provides a theoretical basis for modern, more general models of mantle convection. A priority in adopting the more general models belongs to the Russian scientific school; these models, presently called thermochemical, take into account not only thermal factors but also the mantle convection contribution of chemical heterogeneity of the mantle. Significant analytical results concerning the general models were obtained in the 1970s at the Mechanical–Mathematical Faculty of the Moscow State University and were summarized in the monograph [Myasnikov and Fadeev, 1980]. In particular, these studies provided a rigorous asymptotic derivation of both equations and boundary conditions for a thermochemical model including a boundary layer at the Earth’s surface and a core–mantle transition layer.

The Russian geophysical school has brought forward the concept of generation of lighter mantle material due to its differentiation into metallic and nonmetallic components in the core–mantle transition layer  $D''$  [Artyushkov, 1979; Sorokhtin and Ushakov, 1991]. According to these ideas, the differentiation in the  $D''$  layer is due to melting with a rise in temperature and the descent of molten iron-bearing components of mantle material into the core. The differentiation effect on the mantle convection was studied numerically in [Keondzhyan and Monin, 1980; Monin *et al.*, 1987].

The second impulse to the development of the thermochemical convection concept was given by new computer technologies of seismic data processing. Seismic tomography of deep mantle layers [Dziewonski and Woodhouse, 1987; Fukao *et al.*, 1994] showed that the mantle contains large inclusions of heavy, supposedly eclogitic material that have an important role in the convection process. A new geological paradigm formulated in [Maruyama, 1994] is based on the predominant role of heavy eclogitized masses in the development of mantle convection. However, Maruyama did not verify his paradigm by numerical experiments, and first fragmentary attempts at such modeling were made by Christensen and Yuen [1984].

Thus, initial research of domestic scientists on the thermochemical models, driven by the positive buoyancy force that arises at the core–mantle boundary due to the differentiation processes taking place in its vicinity, was continued by foreign researchers, although their approach was based on the predominant role of the negative buoyancy force arising near the Earth’s surface and associated with the eclogitization of basic rocks of the oceanic crust. As was noted at European conferences of the 1990s on mantle convection and lithospheric dynamics [Van Keken *et al.*, 1997], thermochemical modeling, involving a high degree of resolution, requires much greater computer resources as compared with purely thermal modeling, thereby largely limiting the possibilities of a 3-D numerical simulation.

Numerical modeling provided a fundamental result of great significance for mantle convection [Machetel and Weber, 1991]. Using new experimental data on the endothermic spinel–perovskite phase transition [Ito *et al.*, 1989, 1990] fixing the upper/lower mantle boundary, F. Machetel and P. Weber discovered an intermittent pattern of mantle convection. This removed the basic contradiction between geophysical data the whole-mantle convection scheme for their interpretation and geochemical data that can only be interpreted in terms of convection developing separately in the upper and lower mantle. Later, the intermittent pattern of mantle convection was numerically reproduced by other researchers [Solheim and Peltier, 1994; Tackley *et al.*, 1993], who established that the exothermal olivine–spinel phase transition at a depth of 410 km has an insignificant effect on mantle convection.

Thus, it became clear that, in order to adequately describe mantle convection, modern models should at least include the description of the endothermic phase transition at the upper/lower mantle boundary.

In our work, we attempted to develop and analyze numerically a general thermochemical model of mantle convection incorporating the aforementioned positive and negative forces of chemical buoyancy and the endothermic phase transition.

Since the reliability of inferred results is a critical point in numerical modelling and the probability of numerical errors increases in the case of multifunctional model, we developed and tested our model in several stages. Taking into account the limitations of available computers and the complexity of a mantle convection model incorporating the generation of both heavy and light fractions and the phase transition, we chose a 2-D model of a specific geometry minimizing movement restraints inevitable in the 2-D approach and, on the other hand, simplifying the process of computations.

The traditional axisymmetric 2-D geometry evidently limits the convection pattern to configurations inconsistent with the real geodynamic process and involves a singularity (infinite coefficients) on the symmetry axis, complicating the calculations and deteriorating the accuracy. These limitations could be avoided by considering 2-D flows in the equatorial, rather than meridional, plane.

Our initial calculations modelled the rise of light material to the surface under conditions of thermal convection [Lobkovsky and Kotelkin, 2000a].

Afterward, the endothermic phase transition was included into the purely thermal convection model and, in order to test the model, we reproduced the intermittent mantle convection in terms of axisymmetric geometry. Importantly, the test was successful in relation to both the numerical algorithm and our specific 2-D model geometry [Lobkovsky and Kotelkin, 2000b].

Global thermal eclogitic convection calculated in [Lobkovsky and Kotelkin, 2001] was discussed qualitatively by Japanese authors on the basis of seismic tomography data. These calculations adjusted, on the algorithmic level, the mechanism of eclogite self-generation in lithosphere subduction zones controlled by variations in hydrogeodynamic conditions; i.e. the processes of convection and subduction of the basaltic oceanic crust were made self-consistent, so

that the origination and decay of subduction zones was directly controlled by the process of evolution rather than by a priori artificial postulates of a researcher. As a result, the modelling results agreed well with seismic tomography data.

After these preliminary numerical experiments, we started analysis of the full-scale process of mantle evolution in terms of our thermochemical model. Experiments carried out for a 120° portion of the mantle layer [Lobkovsky and Kotelkin, 2003] demonstrated the possibility of numerical modeling of the mantle evolution whose results are in good agreement with the geological evidence for global cycles that existed throughout the evolution of the Earth. This paper presents results of full-scale modeling of the Earth's evolution for the entire annular layer of the mantle.

## Mathematical Formulation of the Thermochemical Model

### Notation

#### Variables:

$t$ , time;  
 $r, \theta$  and  $\varphi$ , spherical coordinates;  
 $\bar{\mathbf{V}} = (V_r, V_\theta, V_\varphi)$ , velocity;  
 $\Psi$ , stream function for equatorial flows:  $V_r = \partial\Psi/r^2\partial\varphi$ , and  $V_\varphi = -\partial\Psi/r\partial r$ ;  
 $\rho$ , density;  
 $p$ , pressure;  
 $T$ , temperature;  
 $C$ , concentration;  
 $\tau_{r\theta}, \tau_{r\varphi}, \tau_{\theta\theta}$ , and  $\tau_{\theta\varphi}$ , viscous stress components;  
 $\Delta = E + 2\partial/\partial r$  and  $E = \partial^2/\partial r^2 + \partial^2/r^2\partial\varphi^2$ , differential operators;

#### Constants:

$\bar{\mathbf{e}}_r$ , unit vector;  
 $r_e$ , Earth's radius;  
 $r_c$ , radius of the Earth's core;  
 $\rho_0$ , average density;  
 $g$ , gravitational acceleration;  
 $\alpha$ , thermal expansion coefficient;  
 $\kappa$ , thermal diffusivity;  
 $c_p$ , heat capacity;  
 $\eta$ , effective viscosity;  
 $Ch$ , Characteristic, generation rates of heavy and light fractions;  
 $\delta\rho_{\text{ecl}}$ , density jump associated with eclogitization;  
 $\delta\rho_{\text{light}}$ , density jump associated with "demetallization;"

#### Endothermic phase transition parameters:

$\delta\rho_{\text{ph}}$ , phase transition density jump;  
 $\chi(r - r_{\text{ph}})$ , Heaviside function;  
 $r_{\text{ph}}(\varphi)$ , phase transition boundary;  
 $r_{\text{ph}}^0 = 0.875$  (i.e. 670 km), reference position of the phase boundary;

$\gamma$ , slope of the Clapeyron-Clausius phase curve;  
 $h = \gamma \cdot T_{\text{ph}} \cdot \delta\rho_{\text{ph}}/\rho_0^2$ , thermal effect of phase transition;

#### Similarity criteria:

$\text{Ra} = \rho_0 g \alpha T_0 r_e^2 / (\eta v_0)$ , Rayleigh number (the classical value  $\text{Ra}_{1916} = \text{RaPe}$ );  
 $\text{Pe} = r_e v_0 / \kappa$ , Peclet number;  
 $\phi = \delta\rho_{\text{ph}} / \delta\rho_{\text{th}}$ ;  
 $\Gamma = \gamma T_0 / (\rho_0 g r_e) = -dr_{\text{ph}}/dT_{\text{ph}}$ ;  
 $H = \gamma T_{\text{ph}} \delta\rho_{\text{ph}} / (\rho_0^2 T_0 c_p)$ .

The mantle material is regarded as a weakly heterogeneous, highly viscous fluid and is described in the Boussinesq and Stokes approximations; i.e. the medium is considered incompressible and inertialess. The gravitational acceleration is assumed to be constant in the mantle. The density is written as

$$\rho = \rho^0 + \rho', \quad |\rho'| \ll \rho^0, \quad p = p^0 + p', \quad p^0 = \rho^0 \cdot g \cdot (r_e - r),$$

where  $p^0$  is the hydrostatic pressure. We also assume that displacements at a depth of 670 km and the phase boundary slope are small, so that, following Boussinesq, they are approximately taken into account in equations of motion and are neglected the heat conduction equation. In particular, the velocity component normal to the phase boundary is approximated by the radial component  $v_r$ .

The mathematical model consists of the incompressibility condition and equations of motion and heat-and-mass transfer, which in our approximation have the form

$$\begin{aligned} \bar{\nabla} \cdot \bar{\mathbf{V}} &= 0 \\ \bar{\nabla} p' &= -\rho' \cdot g \cdot \bar{\mathbf{e}}_r + \eta \Delta \bar{\mathbf{V}} \\ \partial T / \partial t + \bar{\mathbf{V}} \cdot \bar{\nabla} T &= \kappa \cdot \Delta T + Q \\ \partial C / \partial t + \bar{\mathbf{V}} \cdot \bar{\nabla} C &= Ch \end{aligned} \quad (1)$$

complemented by the relations

$$\begin{aligned} \rho' &= p_{\text{th}} + \rho_{\text{ch}} + \rho_{\text{ph}}, \quad \rho_{\text{th}} = -\rho^0 \cdot \alpha \cdot T, \\ \rho_{\text{ch}} &= -\delta\rho_{\text{ch}} \cdot C, \quad \rho_{\text{ph}} = -\delta\rho_{\text{ph}} \cdot \chi(r - r_{\text{ph}}) \end{aligned} \quad (2)$$

for the thermal, chemical and phase variations in density, respectively, and

$$Q = d\chi/dr \cdot V_r \cdot h / c_p, \quad h = \gamma \cdot T_{\text{ph}} \cdot \delta\rho_{\text{ph}} / \rho_0^2$$

for the heat generation during the endothermic phase transition.

The position of the phase transition is controlled by  $p - T$  conditions. Setting  $|p'| \ll p^0$  at the phase transition depth yields  $p_{\text{ph}} \approx \rho^0 \cdot g \cdot (r_e - r_{\text{ph}})$ , so that  $r_{\text{ph}} = r_{\text{ph}}^0 - \gamma \cdot (T_{\text{ph}} - T_{\text{ph}}^0)$ . The term  $Ch$  describing the generation of the heavy and light fractions is specified below at the stage of numerical calculations.

We introduce the following characteristic scales of the evolutionary process:

$$r_e, v_0, \rho^0, g, T_0, \alpha, \kappa, c_p, \eta, \gamma.$$

$$t_0 = r_e/v_0, \quad p^0 = \rho^0 g r_e, \quad \rho' = \rho^0 \cdot \alpha \cdot T_0 = \delta \rho_{th}.$$

Then, taking into account relations (2), equations (1) can be written in the following dimensionless form:

$$\begin{aligned} \bar{\nabla} \cdot \bar{\mathbf{V}} &= 0 \\ \bar{\nabla} p &= \text{Ra} \cdot (T + C + \phi \cdot \chi) \cdot \bar{\mathbf{e}}_r + \Delta \bar{\mathbf{V}} \\ \frac{\partial T}{\partial t} + \bar{\mathbf{V}} \cdot \bar{\nabla} T &= \frac{\Delta T}{\text{Pe}} + H \cdot \frac{d\chi}{dr} \cdot T \cdot V_r \\ \frac{\partial C}{\partial t} + \bar{\mathbf{V}} \cdot \bar{\nabla} C &= Ch. \end{aligned}$$

The similarity criteria are

$$\text{Ra} = \rho_0 g \alpha T_0 r_e^2 / (\eta v_0), \quad \text{Pe} = r_e \cdot v_0 / \kappa, \quad \phi = \delta \rho_{ph} / \delta \rho_{th},$$

$$\Gamma = \gamma T_0 / (\rho_0 g r_e) = -dr_{ph} / dT_{ph}, \quad H = \gamma T_{ph} \delta \rho_{ph} / (\rho_0^2 T_0 c_p).$$

In what follows, a more general definition of the Rayleigh number through an arbitrary velocity scale is made for a convenient choice of the values  $v_0$  and  $t_0$ ; in this connection, we note the relation  $\text{Ra}_{1916} = \text{RaPe}$ .

Boundary conditions are specified as follows:

$$r = r_c : T = 1, \quad v_r = 0, \quad \tau = 0.$$

$$r = r_e : T = 0, \quad v_r = 0, \quad \tau = 0.$$

To examine the evolution of the mantle layer, initial distributions of temperature and concentration should also be specified.

## Formulation of the Model in an Equatorial Layer With Conical Walls

Numerical experiments were conducted with the use of specific 2-D geometry. The traditional axisymmetric 2-D approach has two drawbacks: first, axisymmetric flows impose serious limitations on the convection pattern that are inconsistent with the real process and, second, coefficients of such a model are infinite on the symmetry axis, complicating calculations and deteriorating their accuracy.

In order to avoid these drawbacks, we consider, using the spherical coordinates  $(r, \theta, \varphi)$ , an equatorial conical layer determined by the conditions  $\pi/2 - \delta < \theta < \pi/2 + \delta$  and assume that its conical boundaries are adiabatic free-slip walls, i.e.

$$\begin{aligned} V_\theta = \tau_{r\theta} = \tau_{\varphi\theta} = \partial T / \partial \theta = \partial C / \partial \theta &= 0 \\ \text{at } \theta = \pi/2 \pm \delta. \end{aligned} \quad (3)$$

The, the model of 2-D equatorial flows, used in [Lobkovsky and Kotelkin, 2000b], are obtained through the passage to the limit  $\delta \rightarrow 0$ . Since conditions (3) are specified on two walls, we obtain in the limit that the conditions

$$\begin{aligned} \partial V_\theta / \partial \theta = \partial \tau_{r\theta} / \partial \theta = \partial \tau_{\varphi\theta} / \partial \theta \\ = \partial^2 T / \partial \theta^2 = \partial^2 C / \partial \theta^2 = 0 \text{ at } \theta = \pi/2 \end{aligned} \quad (4)$$

are also satisfied in the equatorial plane.

Now, in order to obtain the system of equations describing equatorial flows, it is sufficient to write equations in the spherical coordinates  $(r, \theta, \varphi)$ , set  $\theta = \pi/2$  and take into account conditions (3)–(4). Note that, according to the condition  $\partial \tau_{\varphi\theta} / \partial \theta = 0$ , the second derivative  $\partial^2 V_\varphi / \partial \theta^2$  can be represented at  $\theta = \pi/2$  in the form

$$\begin{aligned} \partial^2 V_\varphi / \partial \theta^2 = -V_\varphi \text{ and } \tau_{\theta\theta} = 2\mu \cdot V_r / r \\ \text{at } \theta = \pi/2. \end{aligned} \quad (5)$$

As a result, we obtain the system of equations

$$\begin{aligned} \partial V_r / \partial r + 2V_r / r + \partial V_\varphi / \partial \varphi &= 0 \\ \partial p / \partial r &= \text{Ra} \cdot (T + C + \phi \cdot \chi) + \Delta V_r - 2(\partial V_\varphi / \partial \varphi + V_r) / r^2 \\ \partial p / r \partial \varphi &= \Delta V_\varphi + 2(\partial V_r / \partial r - V_\varphi) / r^2 \\ \partial T / \partial t + V_r \cdot \partial T / \partial r + V_\varphi \cdot \partial T / r \partial \varphi &= \Delta T / \text{Pe} + H \cdot d\chi / dr \cdot T \cdot V_r \\ \partial C / \partial t + V_r \cdot \partial C / \partial r + V_\varphi \cdot \partial C / r \partial \varphi &= Ch, \end{aligned}$$

which contains no singularities and is convenient for numerical modelling. Here  $\Delta$  is the Laplacian,

$$\Delta = E + 2\partial / r \partial r, \quad E = \partial^2 / \partial r^2 + \partial^2 / r^2 \partial \varphi^2.$$

In accordance with the incompressibility condition, we introduce the stream function

$$V_r = \partial \Psi / r^2 \partial \varphi, \quad V_\varphi = -\partial \Psi / r \partial r.$$

By differentiation, we eliminate pressure from the equations of motion and obtain an equation for the stream function:

$$\begin{aligned} 0 = \text{Ra} \cdot (\partial T / \partial \varphi + \partial C / \partial \varphi + \phi \cdot \Gamma \cdot d\chi / dr \cdot \partial T / \partial \varphi) \\ + EE\Psi - 2\partial^2 \Psi / r^2 \partial r^2 + 4\partial \Psi / r^3 \partial r \end{aligned}$$

with the following boundary conditions: at  $r = r_c, r_e$  :  $\Psi = 0$  and  $\tau_{r\varphi} = 0$ , implying that  $\partial^2 \Psi / \partial r^2 = 2\partial \Psi / r \partial r$ . Applying the rule of the differentiation of a composite function, we have

$$\begin{aligned} \partial \chi / \partial \varphi &= d\chi / dr_{ph} \cdot dr_{ph} / dT_{ph} \cdot \partial T_{ph} / \partial \varphi \\ &= (-d\chi / dr) \cdot (-\Gamma) \cdot \partial T_{ph} / \partial \varphi. \end{aligned}$$

A disadvantage of this model of equatorial flows is the impossibility of its solution beyond the walls into the entire spherical layer of mantle. However, in this case it is basically more important that the numerically modelled flows can be realized in physical simulation models with small apex angles  $\delta$ .

## Numerical Implementation of the Model

In numerical implementation, the model differential equations were approximated, within the second-order accuracy,

by finite difference relations on meshes regular in the coordinates  $r$  and  $\varphi$ . The maximum size of meshes used in our calculations amounted to  $256 \times 2048$  cells covering the area ( $0.5 \leq r \leq 1$ ;  $0 \leq \varphi \leq 2\pi$ ), which yields a cell of the size ( $dr \approx 12$  km;  $d\varphi \approx 0, 14^\circ$ ). The integration of the heat-and-mass transfer equations over time was also performed within a second order of accuracy.

The concentrated force and heat generation associated with the phase transition and described by the value  $d\chi/dr$  were referred to the nondisturbed position of the phase boundary  $r_{\text{ph}}^0 = 0.875$  and were distributed (approximated) over the thickness of one mesh layer.

The generation of heavy and light fractions was also modelled at individual nodes, i.e. was accurate to steps in space and time. Eclogites could only be generated at depths of 80–100 km. Moreover, the generation of eclogites could take place only at nodes that were adjacent to the subducting boundary of convective cells ( $\Psi = 0$ ,  $Vr < 0$ ) at the current time moment. Under the conditions mentioned above, the concentration at a node assumes the value  $C_{\text{ecl}}$ , and the further dynamics of eclogite is determined by the heat-and-mass transfer equation.

Generation of the lighter fraction can only occur at nodes adjacent to the lower boundary of the model domain, where heavier iron-bearing fractions can sink into the core. Moreover, the lighter fraction forms only if the temperature of the cell at a current time moment exceeds the melting temperature  $T_{\text{melt}}$ , and in this case the concentration assumes a value  $C_{\text{light}}$ .

Thus, the numerical model of the mantle is completely self-consistent: the differentiation in the D'' layer is controlled by temperature, the number and position of subduction zones is directly determined by the hydrodynamic conditions in the upper mantle, and all processes, including the phase transition, are interrelated through the velocity field.

The initial temperature distribution was taken in the form

$$t = 0; T(r) = 1 - \exp[A \cdot (r - 1)].$$

Choosing the value  $A = 16$ , we obtain the initial distribution close to that recommended in [Vityazev, 1990].

Small initial perturbations causing the mantle to depart from the equilibrium state were furnished by a small amount of light material (6%) uniformly distributed throughout the mantle in a random manner. Eclogites are absent at the initial time moment. The initial distribution of temperature and concentration are shown in the first frame of the animated experiment (see also Figure 2.0a below). Note that, in the inertialess approximation, the velocity field is determined at any (including initial) time moment by the temperature and concentration distributions. With initial distributions specified in this way, numerical experiments showed that 3- and 4-mode patterns of initial convection (the initial number of ascending and descending flows, i.e. oceans and continents) are most probable.

Many numerical experiments were carried out with various initial conditions, model similarity criteria ( $Ra$ ,  $Pe$ ,  $\phi$ ,  $\Gamma$  and  $H$ ) and parameters controlling the chemical transformation rate  $Ch$ .

The main goal of our study was to constrain the values of constitutive parameters at which the thermochemical model

of the Earth's global evolution fits best the data of historical geology. The numerical experiments revealed the presence of a relatively narrow range of values of constitutive parameters in which the mantle evolution exhibits a well-expressed pattern involving a set of different cycles; it is noteworthy that this range is consistent with the available published data on physical properties of the mantle.

Temperature distributions were visualized on computer display in a natural color palette convenient for perception; inclusions of eclogite and lighter material are superimposed on the temperature distribution and their common dynamics is animated. The results shown in this paper were obtained with the following values of dimensionless parameters:

$$Ra = 5 \cdot 10^4, Pe = 1300, \phi = 2, \Gamma = -0.06, H = -0.035,$$

$$C_{\text{ecl}} = -0.3, T_{\text{melt}} = 0.9, C_{\text{light}} = 1.0.$$

The corresponding dimensional values are

$$t_0 = 1 \text{ Gyr}, v_0 = 0.7 \text{ cm/yr}, T_0 = 4000^\circ\text{C},$$

$$\rho^0 = 4200 \text{ kg m}^{-3}, g = 10 \text{ m s}^{-2},$$

$$r_e = 6.4 \times 10^6 \text{ m}, r_c = 0.5 \times r_e;$$

$$\kappa = 10^{-6} \text{ m}^2 \text{ s}^{-1}, \alpha = 1.4 \times 10^{-5} \text{ 1/}^\circ,$$

$$c_p = 1.25 \times 10^3 \text{ J/(kg }^\circ\text{)};$$

$$\delta\rho_{\text{th}} = 200 \text{ kg m}^{-3}, \delta\rho_{\text{ph}} = 400 \text{ kg m}^{-3},$$

$$\delta\rho_{\text{ecl}} = 200 \text{ kg m}^{-3}, \delta\rho_{\text{light}} = 600 \text{ kg m}^{-3};$$

$$\eta = 10^{22} \text{ kg m}^{-1} \text{ s}^{-1} \text{ and } \gamma = -4 \text{ MPa/}^\circ.$$

## Results

With the aforementioned values of constitutive parameters, the numerical modelling results correlate remarkably well with main stages of the Earth's evolution. The main modelling result is presented in Figure 1, showing the variation in the average velocity of the mantle, i.e. the convection activity variation during 7.6-Gyr evolution (85000 time steps of integration), and variations in the average temperatures of the upper, lower and whole mantle, which are the main consequences of the convective dynamics. Detailed (non-averaged) variations in temperature and concentrations of eclogite and lighter material during 3.8 Gyr of the Earth's geological history are presented as the video file *Mantle.avi*, divided into four parts for its easier examination via Internet. Figure 2 presents detailed distributions of temperature and admixtures, as well as hydrodynamic patterns corresponding to the key events of mantle history (peaks in Figure 1).

Figure 1 and the videorecord of the experiment show that the geodynamic process, "launched" from its unstable initial state 3.8 Gyr ago, reached a maximum velocity of about 30 cm/yr, after which it rapidly attained the stable state of slow long-term evolution followed by global cycles, the first four of which correlate well with geological data on the development of the Wilson cycles. In agreement with

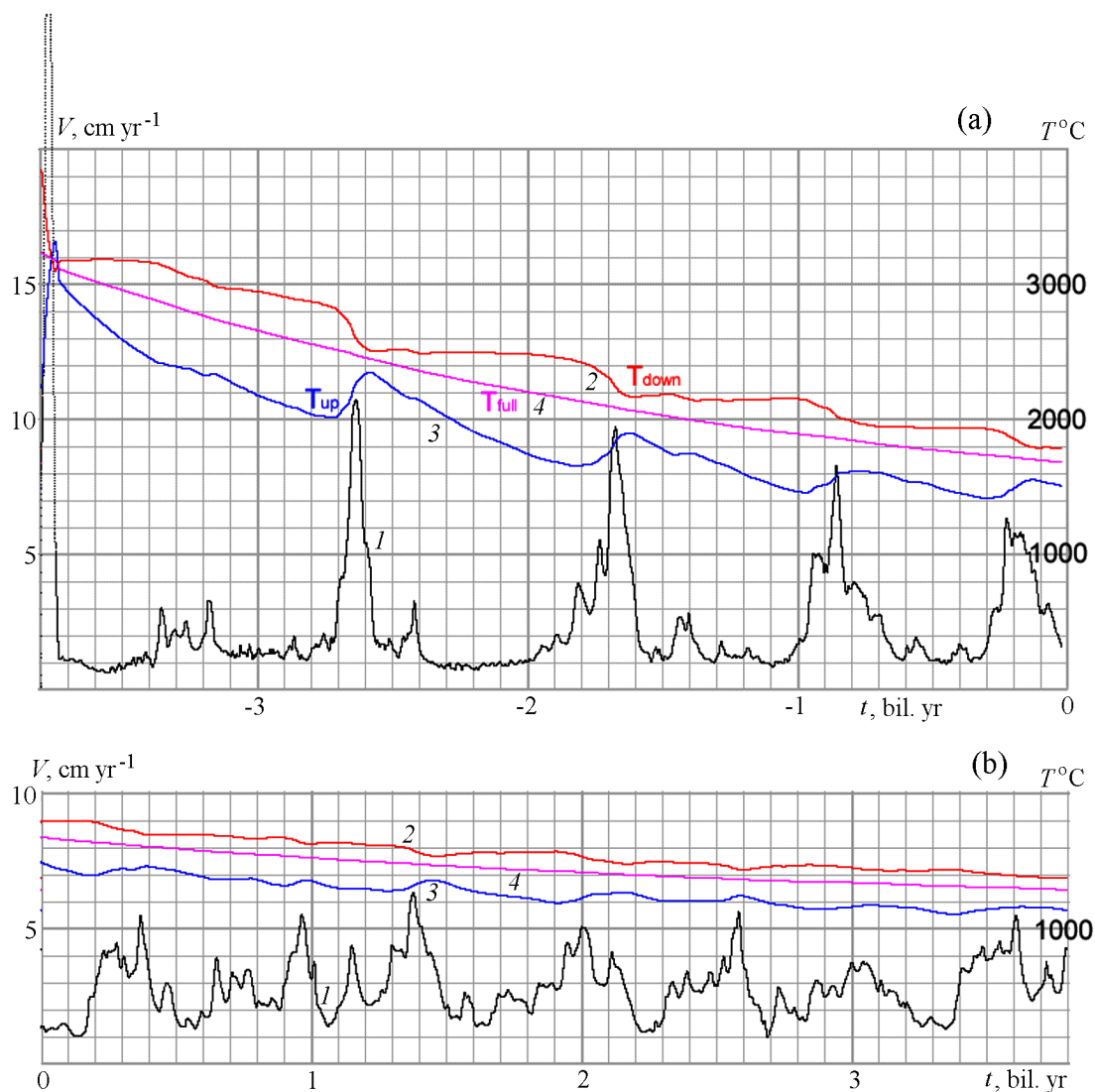


**Figure 1.** Geodynamic activity and temperature variation: (a) the past: Wilson global cycles; (b) the future: degeneration of the global cycles. The black curve (1) is the average mantle velocity, the red curve (2) is the average temperature of the lower mantle, the blue curve (3) is the average temperature of the upper mantle, and the violet curve (4) is the average temperature of the whole mantle.

the geological history [Khain, 2001], the numerical experiment yields an initial intense thermal wave coming from the planet's interior followed by the long-term epoch of Archean evolution; the subsequent activity pulse correlate with the existence and breakup of the first epi-Archean continent in the period from 2.3 to 2.6 Ga; further pulses coincide in time with the second epi-Paleoproterozoic supercontinent existing from 1.65 to 1.4–1.35 Ga, the third epi-Mesoproterozoic supercontinent Rodinia (1–0.8 Ga) and, finally, the Wegener's Pangea (320–200 Ma).

The validity of such an interpretation of the dynamic evolution shown in Figure 1, according to which outbursts of geodynamic activity play a key role in the geological history of the Earth, becomes evident from analysis of the video-record of the experiment. Figure 2 presents fragments of

virtual hydrodynamic evolution of the Earth's mantle illustrating its characteristic features. Compare the states of the mantle layer before (Figure 2a), during (Figure 2b) and after (Figure 2c) an activity pulse responsible for a change in global cycles. Fluid dynamics patterns are shown by streamlines at the bottom of Figure 2 (shades of yellow and green show clockwise and counterclockwise motions, respectively, and the stream function is normalized to the current average velocity), and the distributions of thermochemical heterogeneities for these flow patterns are shown at the top.

Figure 2.0 shows the initial state of the mantle in accordance with the postulated post-accretionary state of the planet. This is a metastable thermal state with uniformly distributed random inclusions of light material, with no eclogite being present. The heterogeneities produce weak

small-scale convection evolving, in accordance with hydrodynamic laws, into rapidly growing (in the given case, 4-mode) whole-mantle convection, leading to an abrupt mantle overturn (an ideal overturn) characterized by velocities and surface heat fluxes that are highest in the history of the Earth. As a result, the mantle passes into a stable heterogeneous state, opening the long period of the Archean evolution.

The post-Archean overturn (Figure 2.1), occurring in a 2-mode regime and characterized by smaller velocities, gives rise to asymmetry of the mantle layer, so that subsequent overturns occur in a unimodal regime (Figures 2.2–2.4). As seen from Figure 2, long intervals between geodynamic activity peaks are characterized by relatively slow mantle flows with average velocities of 1–2 cm/yr (see Figure 1) in the regime of two-layer mantle convection, when heavier and lighter heterogeneities accumulate on opposite sides of the phase boundary (see Figure 2a). Several plumes and regional-scale subducting downflows are observed in the upper and lower mantle.

However, the geodynamic activity outbursts, observable in Figure 1a as narrow peaks of the average velocity of mantle flows reaching  $\sim 10$  cm/yr (which is typically three times lower than the maximum velocities), occur within the framework of predominantly whole-mantle convection, as is evident from Figure 2b; this regime exists usually (but not always) for a long time (Figure 1b).

## Discussion

Examination and analysis of videorecords of numerous modelling experiments provides insights into the origin and nature of the observed patterns. Note that our model does not include the internal heating due to radioactive sources; neither does it include the cooling of the Earth's core. This study examined the mantle evolution from an initial state that is much hotter than its final state. The mantle evolution proceeds in an impulsive, rather than quasi-stationary, manner due to the presence of the endothermic barrier associated with the phase transition at a depth of 670 km. The Wilson cycle essentially reduces to the fact that, over a certain time of two-layer convection (the period of the Wilson cycle), the thinner upper mantle cools first because its cooling surface is four times larger than the heating surface of the lower mantle. If the cooling of the upper mantle were uniform, the phase barrier would have been overcome simultaneously throughout the boundary, resulting in a complete replacement of the upper mantle material (an ideal overturn). The Bertrand cycles would have been absent in this case.

The presence of lateral heterogeneities, first of all, accumulations of heavy subducting material leads to “premature” local flows of the phase barrier; yet, due to an insufficient external energy supply, such flows cannot exist for a long time and the homogeneity of the upper mantle is restored. The recurrence rate of these events (Bertrand cycles) depends on the relation between the height of the phase barrier and the accumulation rate of heavy material. Similar

processes of the accumulation of lighter material take place on the opposite side of the phase boundary.

The evolution pattern is basically different, if a local flow through the phase boundary occurs in the case of a cold upper and hot lower mantle. Vigorous whole-mantle convection developing in this case rapidly replaces the cold upper mantle material with the hot lower mantle material. Such mantle overturns differ from “normal” avalanches by considerable lateral displacements of mantle material; indeed, before the heavy material of upper mantle will sink into the lower mantle, it should be horizontally transported over a distance equal to about one-fourth of the equator length. For this reason, overturns radically change the Earth's face and are natural landmarks of the geological history. It is unimodal overturns that are responsible for the asymmetric distribution of continents and oceans. The average temperature of the upper mantle rises, over the overturn time, by a few tens of degrees (by a few hundreds of degrees during the earliest overturns), and the lower mantle temperature accordingly decreases. However, the average temperature of the whole mantle is insensitive to both overturns and avalanches, smoothly decreasing by an exponential law.

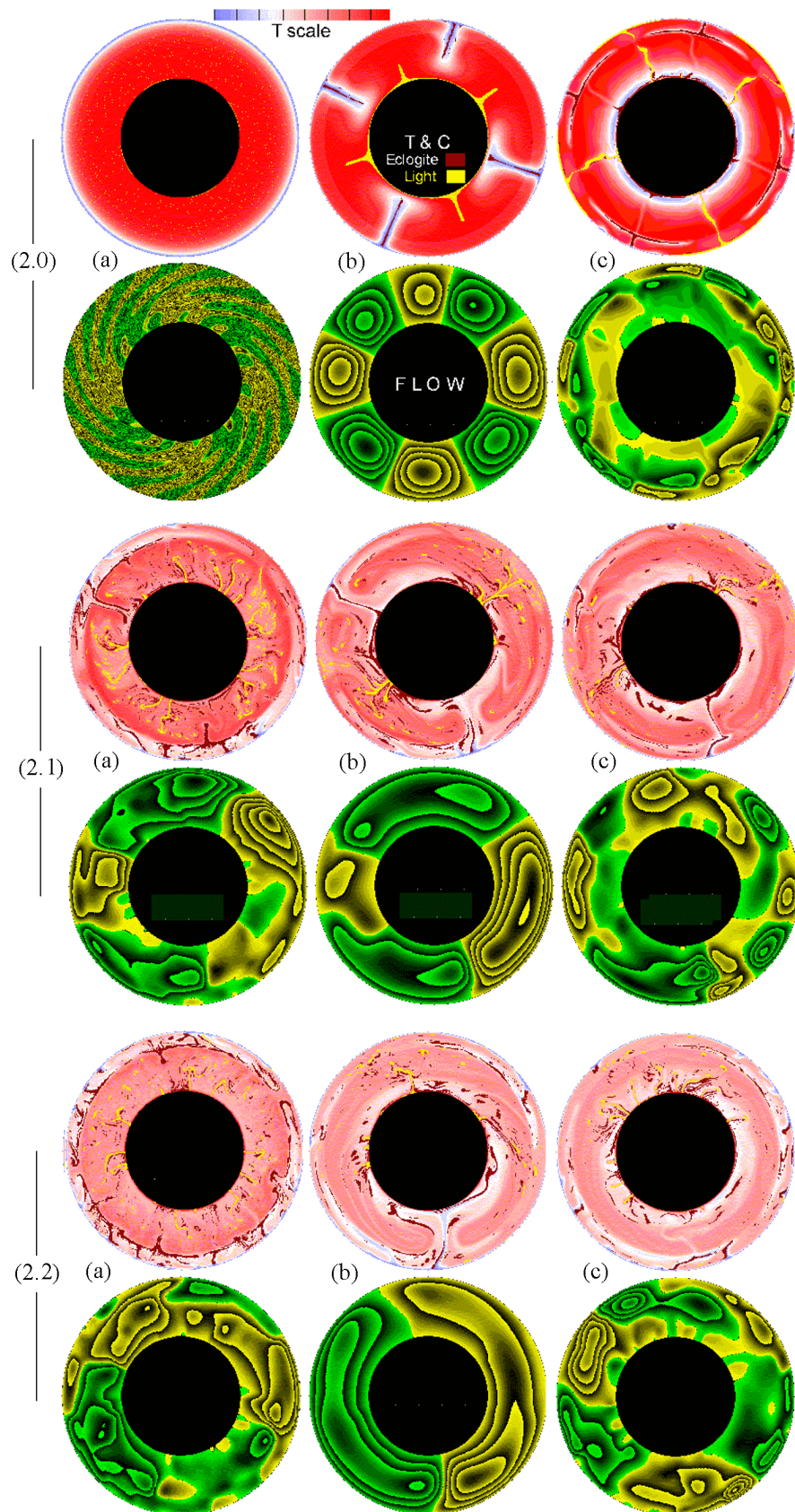
A factor having important implications for the appearance of mantle overturns is the starting impulse initiating the convective process and determining its behavior at the initial stage of the evolution (a few billion years). In the experiment, illustrated above, such a concentrated starting impulse is ensured by a post-accretionary planetary state uniform in the angular coordinate and unstable in its radial component.

Numerical experiments show that mantle overturns (and Wilson cycles) degenerate with time into avalanches, typically through the breakdown of a concentrated pulse into a series of avalanches.

Between phase boundary breakthroughs, developed unsteady-state thermochemical convection takes place in both upper and lower mantle, and its main events are reorganizations of convective cells. Small cells unite to form larger ones, which is well observable as convergence of subduction zones in the upper mantle and as convergence of uprising plumes in the lower mantle. During such convergence, flow velocities increase for a time, giving rise to small pulsations superimposed on the averaged process; however, large cells rapidly exhaust their feeding sources and break up into smaller and weaker cells, which is clearly indicated by new subduction zones in the upper mantle. These events regularly recur and should be associated with the Stille cycles. They are primarily governed by hydrodynamic laws but are additionally enhanced by eclogitization of the oceanic crust. Note that, along with the Stille cycles observed at the Earth's surface, similar recurrent processes associated with the development of plumes take place in the lower mantle.

## Conclusion

We are well aware that the results, presented in this paper and obtained within the framework of a rather simple model



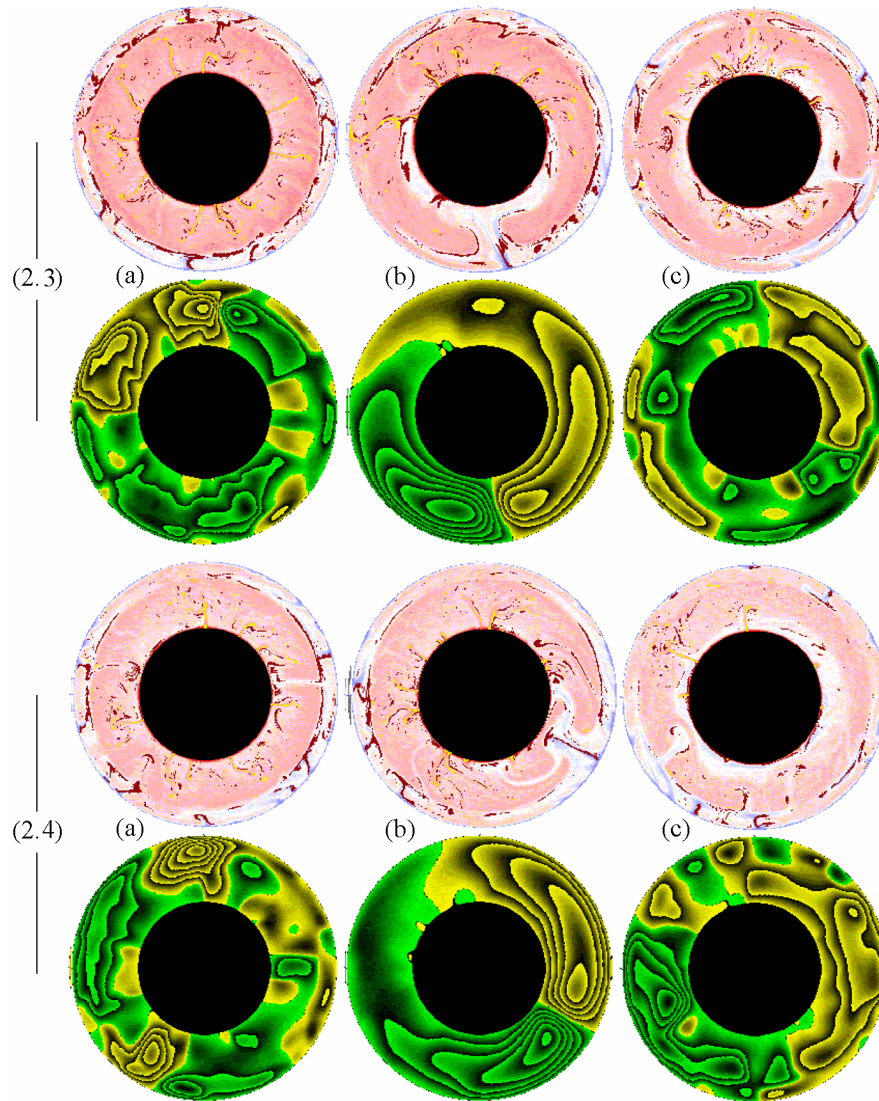


**Figure 2.** Key points in the Earth's history: mantle overturns. (2.0) Post-accretionary state and the convection onset, (2.1) Formation of a pair of epi-Archean supercontinents, (2.2) Formation of an epi-Paleoproterozoic supercontinent, (2.3) Formation of the epi-Mesoproterozoic supercontinent Rodinia, (2.4) Formation of the Wegener's Pangea.

Each event is represented by three states: (a) end of the global state: unstable state of the mantle (2.0a, initial state); (b) change of global cycles: mantle overturns; (c) beginning of the global cycle: stable thermochemical state. Each state is characterized by distributions of temperature and admixtures, shown at top of a figure, and by a distribution of streamlines, shown at the bottom (lines of the same color; yellowish and greenish tints indicate clockwise and counterclockwise motions, respectively).

of the mantle, characterize only a possible hypothetical variant of the real terrestrial process. Moreover, we should note that the “convincing” experiment described above is an exceptional case among all experiments that we conducted. Due to the stochastic nature of the process, the smallest changes in the modelling conditions shift peaks of the resulting curve, worsening their agreement with the evidence of historical geology; some peaks become diffused and degenerate into series of avalanches. However, the experiment presented in this paper and our treatment of the Earth's

evolution reflect, on a statistical level, average tendencies of a large number of experiments.

## References

- Artyushkov, E. V. (1979), *Geodynamics*, 320 pp., Nauka, Moscow.  
 Bercovici, D., G. Schubert, and G. A. Glatzmaier (1989), Three-dimensional spherical models of convection in the Earth's mantle, *Science*, *244*, 950–955.

- Christensen, U. R., and D. A. Yuen (1984), The interaction of a subducting lithospheric slab with a chemical or phase boundary, *J. Geophys. Res.*, *89*, 4389–4402.
- Dziewonski, A. M., and J. H. Woodhouse (1987), Global images of the Earth's interior, *Science*, *236*, 37–48.
- Fukao, Y., S. Maruyama, M. Obayashi, and H. Inoue (1994), Geologic implication of the whole mantle *P* wave tomography, *J. Geol. Soc. Japan*, *100*(1), 4–23.
- Glatzmaier, G., G. Schubert, and D. Bercovici (1990), Chaotic, subductionlike downflows in a spherical model of convection in the Earth's mantle, *Nature*, *347*, 274–277.
- Ito, E., and T. Takahashi (1989), Postspinel transformations in the system  $Mg_2SiO_4$ – $Fe_2SiO_4$  and some geophysical implications, *J. Geophys. Res.*, *94*, 10,637–10,646.
- Ito, E., M. Akaogi, L. Topor, and A. Navrotsky (1990), Negative pressure-temperature slopes for reactions forming  $MgSiO$  perovskite calorimetry, *Science*, *249*, 1275–1278.
- Jeanloz, R., and A. B. Thompson (1983), Phase transitions and mantle discontinuities, *Rev. Geophys.*, *21*, 51–74.
- Keondzhyan, V. P., and A. S. Monin (1980), On the chemical convection in the Earth's mantle, *Dokl. Akad. Nauk SSSR* (in Russian), *253*(1), 78–81.
- Khain, V. E. (2001), Large-scale cyclicity, its possible origins and general tendencies of the Earth's tectonic history, in *Fundamental Problems of General Tectonics* (in Russian), pp. 403–424, Nauchnyi Mir, Moscow.
- Lobkovsky, L. I., and V. D. Kotelkin (2000a), Geodynamics of mantle plumes, their interaction with asthenosphere and lithosphere, and their effects on rifting and trap formation, in *General Problems of Tectonics: Tectonics of Russia* (in Russian), pp. 304–308, GEOS, Moscow.
- Lobkovsky, L. I., and V. D. Kotelkin (2000b), A two-layer thermochemical model of mantle convection and its geodynamic implications, in *Problems of Global Geodynamics: Proceedings of the OGGGGN RAN Theoretical Seminar of 1998–1999* (in Russian), edited by D. V. Rundkvist, pp. 29–53, GEOS, Moscow.
- Lobkovsky, L. I., and V. D. Kotelkin (2001), Intermittent thermal eclogitic convection in mantle incorporating the 670-km phase transition and its comparison with data of seismic tomography, in *Tectonics of Neogea: Global and Regional Aspects* (in Russian), pp. 378–381, GEOS, Moscow.
- Lobkovsky, L. I., and V. D. Kotelkin (2003), Numerical modeling of the Earth's global evolution during 4 Gyr in terms of a thermochemical model of mantle convection, in *Tectonics and Geodynamics of the Continental Lithosphere* (in Russian), pp. 352–357, GEOS, Moscow.
- Machetel, F., and P. Weber (1991), Intermittent layered convection in a model mantle with an endothermic phase change at 670 km, *Nature*, *350*, 55–57.
- Maruyama, S. (1994), Plume tectonics, *J. Geol. Soc. Japan*, *100*(1), 24–49.
- Monin, A. S., D. G. Seidov, O. G. Sorokhtin, and Yu. O. Sorokhtin (1987), Numerical modeling of mantle convection, *Dokl. Akad. Nauk SSSR* (in Russian), *294*(1), 58–63.
- Monin, A. S., D. G. Seidov, O. G. Sorokhtin, and Yu. O. Sorokhtin (1987), Numerical modeling of mantle convection patterns, *Dokl. Akad. Nauk SSSR* (in Russian), *295*(5), 1080–1083.
- Myasnikov, V. P., and V. E. Fadeev (1980), *Evolutionary Models of the Earth and Terrestrial Planets* (in Russian), VINITI, Moscow.
- Solheim, L., and W. Peltier (1994), Avalanche effects in phase transition modulated thermal convection: A model of Earth's mantle, *J. Geophys. Res.*, *99*(B4), 6997–7018.
- Sorokhtin, O. G., and S. A. Ushakov (1991), *Global evolution of the Earth*, 446 pp., MSU, Moscow.
- Tackley, P., D. Stevenson, G. Glatzmaier, and G. Schubert (1993), Effects of an endothermic phase transition at 670 km depth in a spherical model of convection in the Earth's mantle, *Nature*, *361*, 699–704.
- Trubitsyn, V. P., and V. V. Rykov (1998), Three-dimensional spherical models of mantle convection, continental drift, and formation and breakup of supercontinents, *Russian J. Earth Sci.*, *1*(2).
- Trubitsyn, V. P., and V. V. Rykov (2000), Mantle convection with floating continents, in *Problems of Global Geodynamics: Proceedings of the OGGGGN RAN Seminar of 1998–1999* (in Russian), edited by D. V. Rundkvist, pp. 7–28, GEOS, Moscow.
- Van Keken, P. E., S. D. King, H. Schmeling, U. R. Christensen, D. Neumeister, and M.-P. Doin (1997), A comparison of methods for the modeling of thermochemical convection, *J. Geophys. Res.*, *102*(B10), 22,477–22,495.
- Vityazev, A. V. (1990), Early Evolution of the Earth, *Zemlya i Vselennaya* (in Russian), (2), 18–24.

---

L. I. Lobkovsky, P. P. Shirshov Institute of Oceanology, RAS  
 V. D. Kotelkin, Mechanical–Mathematical Faculty of the Moscow State University, Leninskiye Gory, Moscow, 119992, Russia

(Received 22 March 2004)